8-22-2017

Molecular Basis for the Substrate Specificity of Quorum Signal Synthases

Shi-Hui Dong
University of Illinois at Urbana-Champaign

Nicole D. Frane
Boise State University

Quin H. Christensen
University of Washington

E. Peter Greenberg
University of Washington

Rajesh Nagarajan
Boise State University

See next page for additional authors

Molecular basis for the substrate specificity of quorum signal synthases

Shi-Hui Dong[a,d], Nicole D. Frane[b], Quin H. Christensen[c,1], E. Peter Greenberg[c], Rajesh Nagarajan[b], and Satish K. Nair[a,d,e,2]

[a]Department of Biochemistry, University of Illinois at Urbana–Champaign, Urbana, IL 61801; [b]Department of Chemistry and Biochemistry, Boise State University, Boise, ID 83725; [c]Department of Microbiology, University of Washington, Seattle, WA 98195; [d]Institute for Genomic Biology, University of Illinois at Urbana–Champaign, Urbana, IL 61801; and [e]Center for Biophysics and Computational Biology, University of Illinois at Urbana–Champaign, Urbana, IL 61801

Edited by Jerrold Meinwald, Cornell University, Ithaca, NY, and approved July 14, 2017 (received for review March 31, 2017)

In several *Proteobacteria*, LuxI-type enzymes catalyze the biosynthesis of acyl–homoserine lactones (AHL) signals using *S*-adenosyl–L-methionine and either cellular acyl carrier protein (ACP)-coupled fatty acids or CoA–aryl/acyl moieties as progenitors. Little is known about the molecular mechanism of signal biosynthesis, the basis for substrate specificity, or the rationale for donor specificity for any LuxI member. Here, we present several cocrystal structures of BjaI, a CoA-dependent LuxI homolog that represent views of enzyme complexes that exist along the reaction coordinate of signal synthesis. Complementary biophysical, structure–function, and kinetic analysis define the features that facilitate the unusual acyl conjugation with *S*-adenosylmethionine (SAM). We also identify the determinant that establishes specificity for the acyl donor and identify residues that are critical for acyl/aryl specificity. These results highlight how a prevalent scaffold has evolved to catalyze quorum signal synthesis and provide a framework for the design of small-molecule antagonists of quorum signaling.

quorum sensing | homoserine lactone | crystallography

Bacteria can engage in a form of cell-to-cell communication called quorum sensing via the synthesis and subsequent perception of chemical signals (1, 2). Quorum sensing allows for the coordination of gene expression in response to changes in population density and is used by many bacterial species to regulate behaviors such as motility, virulence, and antibiotic production (3). For example, quorum sensing modulates maturation of the protective biofilm that provides immune and antibiotic resistance in the opportunistic pathogen *Pseudomonas aeruginosa* (4, 5), regulates the biosynthesis of an exopolysaccharide virulence factor in the plant pathogen *Pantoea stewartii* (the causative agent for Stewart's Wilt disease) (6), and is involved in the control of swimming and swarming motility in the zoonotic agent *Yersinia enterocolitica* (7). Disruption of quorum signaling by either natural or synthetic means is shown to be detrimental to bacterial pathogenicity, without causing lethality (8).

All known quorum-signaling networks use three critical components: a means for generating the signal (known as autoinducers), receptors that can detect the signal, and a regulator of genes, generally including those for the production of the signal itself (positive feedback loop) (9). Bacteria can intracellularly synthesize their cognate autoinducer, which is then released into the surrounding environment in a passive or active manner (10, 11). The environmental concentration of the inducer grows with an increase in population density, until above a "quorate" threshold at which the corresponding concentration of inducer induces a coordinated response in gene expression by activation of the signal receptor (12).

Commonly used signals among many species of *Proteobacteria* consist of cell-permeable fatty acyl–homoserine lactones (13). The acyl chain lengths of these molecules vary between 4 and 18 carbons and also differ in backbone saturation and/or oxidation state at the β-carbon, depending on the specific quorum-signaling system (2). Dedicated LuxI family member *N*-acyl–homoserine lactone (AHL) synthases produce these signaling molecules (14). At signal levels that exceed the threshold concentration for perception by the LuxR transcriptional response regulators, the LuxR–signal complex regulates the expression of the genes in the corresponding regulon (15). Both the LuxI AHL synthase and LuxR signal receptor show specificity for their cognate AHL signal, and different signals are generated and perceived by specific, independent proteins (13).

To date, three different AHL synthase classes have been identified, including the LuxI (12), LuxM/AinS (16, 17), and HdtS families (18). The identification of HdtS from *Pseudomonas fluorescens* as an AHL synthase is tenuous and based on in vitro experiments using recombinant protein (19). Of these different classes, the LuxI synthase from *Vibrio fischeri* was the first to be identified, and the LuxI family is among the most widespread and the most widely studied. LuxI synthases catalyze the transfer of an acyl group bound to acyl carrier protein (ACP) from fatty acid biosynthesis to *S*-adenosyl–L-methionine (SAM) (20, 21). Kinetic studies of RhlI, a LuxI-type AHL synthase from *P. aeruginosa*, are consistent with a sequential ordered mechanism with SAM binding before the acyl–ACP (22). The acyl transfer reaction yields an acyl–SAM intermediate, which then undergoes lactonization to form the *N*-acyl–homoserine lactone.

Analysis of signals produced by the soil bacterium *Bradyrhizobium japonicum* identified the branched fatty acyl-derived isovalerate–homoserine lactone as a signal produced by the LuxI homolog BjaI and perceived by the BjaR receptor (23). Importantly, BjaI is demonstrated to exclusively use isovaleryl–CoA as a substrate, and no activity could be detected using isovaleryl–ACP. Sequence analysis of BjaI with the other CoA-dependent synthases, RpaI (which generates *p*-coumaroyl–homoserine lactone) (24) and BraI (generates *p*-cinnamoyl–homoserine lactone) (25), shows that these enzymes are closely related to each other (~50% sequence identity) and only distantly related to ACP-dependent LuxI enzymes (~30% sequence identity) (26).

Since the first identification of the *V. fischeri* LuxI nearly two decades ago, AHL synthases have been subject to extensive genetic, biochemical, and biotechnological investigations (17, 27). However, detailed mechanistic characterization has been limited

Significance

These first structures of a homoserine-lactone quorum-signal synthase bound to various substrates and analogs help to provide a molecular rationale for understanding acyl chain specificity. Based on the structural data, we show how different clades of signal synthases can accommodate their cognate acyl–CoA ligands. Lastly, the elucidation of the reaction mechanism for the signal synthase may provide a rationale for the design of therapeutic small-molecule antagonists.

Author contributions: S.K.N. designed research; S.-H.D., N.D.F., R.N., and S.K.N. performed research; S.-H.D., Q.H.C., and E.P.G. contributed new reagents/analytic tools; Q.H.C. suggested experiments; S.-H.D., N.D.F., R.N., and S.K.N. analyzed data; and S.K.N. wrote the paper.

The authors declare no conflict of interest.

This article is a PNAS Direct Submission.

Data deposition: Crystallography, atomic coordinates, and structure factors [accession nos. 5W8D (BjaI-MTA), 5W8G (BjaI-SAH), 5W8C (BjaI-IVCoA-MTA), 5W8A (BjaI-IPCoA-SAM), and 5W8E (BjaI-IV-SAH)].

[1]Current address: BlueBird Bio, Cambridge, MA.

[2]To whom correspondence should be addressed. Email: snair@illinois.edu.

This article contains supporting information online at www.pnas.org/lookup/suppl/doi:10.1073/pnas.1705400114/-/DCSupplemental.

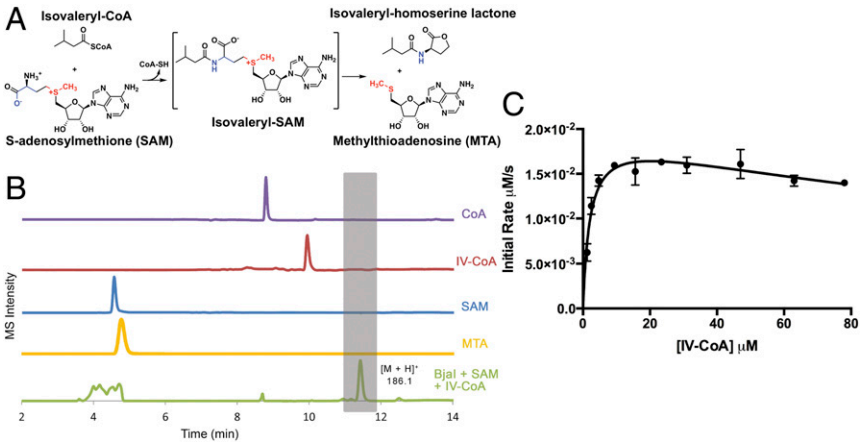

Fig. 1. The AHL synthase reaction mechanism. (*A*) Overall reaction scheme showing the BjaI-catalyzed production of isovaleryl–AHL from isovaleryl–CoA and *S*-adenosylmethionine via a presumptive isovaleryl–SAM intermediate. (*B*) Formation of isovaleryl–AHL analyzed by HPLC analysis (green trace). The elution profiles for the isolated standards are shown in the panels above. (*C*) Michaelis–Menten curve obtained by measuring CoA production over varying concentrations of isovaleryl–CoA (IV-CoA), at a fixed concentration of 300 μM *S*-adenosylmethionine. The slight decrease in initial rate may be due to substrate inhibition, which has previously been observed for ACP-dependent AHL synthases (31).

due to a lack of structure–function studies of any LuxI member with cognate substrates. Unliganded structures of the acyl–ACP-dependent LuxI enzymes, *P. aeruginosa* LasI [producing 3-oxo–C12 homoserine lactone (HSL)] (28) and *Pantoea stewartii* EsaI (producing 3-oxo–C8 HSL) (29), identify the overall fold of these enzymes. Recent cocrystal structures of *Burkholderia glumae* TofI (producing C8 HSL) identified a small-molecule ligand-binding pocket (30), but the physiological relevance of the pocket is unclear.

Here, we present detailed biochemical and kinetic studies of BjaI from *B. japonicum*, along with several high-resolution crystal structures of complexes with substrate analogs, products, and a covalent isovaleryl–SAH intermediate that does not undergo lactone formation. Steady state kinetic analysis of structure-guided site-specific variants provides insights into the role of active-site residues in catalysis. These combined data provide a molecular framework for nearly two decades worth of prior results of a reaction mechanism that is unique among other enzymes that use SAM.

Results

Kinetic Characterization of Recombinant BjaI. Prior mass spectrometric analysis of metabolites from cultured supernatants of *B. japonicum* demonstrated activation of quorum signaling with isovaleryl–CoA (23), consistent with gene regulation induced through the formation of an isovaleryl–homoserine lactone (Fig. 1*A*). Purified, recombinant BjaI can catalyze the formation of the AHL signal using isovaleryl–CoA and *S*-adenosylmethionine as substrates (Fig. 1*B*). To determine the kinetic parameters for wild-type and site-specific variants of BjaI using isovaleryl–CoA as a substrate, we used a colorimetric assay developed by Tipton and colleagues (Fig. 1*C*) (22). The enzyme carried out acylation of SAM with catalytic efficiency (k_{cat}/K_m) of 2.14×10^4 M^{-1} s^{-1}, which is a consequence of the slow turnover number (k_{cat}). The catalytic efficiency is within an order of magnitude to that observed for ACP-dependent AHL synthases, such as RhlI (22) and BmalI (26), with the appropriate ACP-linked substrate, and is consistent with a lack of selection for catalytic efficiency due to the small concentration of produced signal that is required (25). Kinetic parameters for BjaI and each of the active-site variants can be found in Table 1.

Determination of Substrate Scope. We chemically synthesized a panel of branched acyl–CoA substrates and tested each of these as substrates for the production of the corresponding AHL (Fig. 2*A* and *SI Appendix*, Figs. S1–S12). BjaI was relatively tolerant for the acyl donor and could accommodate longer substrates, including the C6-branched methylvaleryl–CoA and the C7-branched methylhexanoyl–CoA, as well as the shorter C4-branched isobutyryl–CoA (Fig. 2*B*). This latter substrate is shortened by one methylene relative to isovaleryl–CoA and was not as efficiently used by BjaI as the longer substrates up to methylhexanoyl–CoA. In contrast, branched chains that were longer than C8 (i.e., neodecanoyl–CoA) were not substrates for the enzyme. These data suggest that the acyl-binding pocket for BjaI can use a range of branched substrates of length consisting of up to, but not exceeding, C7. To further delineate acyl chain length tolerance, we determined the kinetic parameters of BjaI against a panel of eight different acyl–CoAs (*SI Appendix*, Table S1). Catalytic efficiency was notably compromised as the linear acyl chain length increased or decreased, and no synthase activity could be detected using acyl chains of length C8 or longer. Notably, for BjaI substrates, chain length was more critical than the presence of branching, as butyryl–CoA was used ∼3.5 times better than isobutyryl–CoA. These data all indicate the BjaI can catalyze the production of AHL using acyl–CoA substrates within the range of four to six carbons, albeit with much lower catalytic efficiency than with isovaleryl–CoA.

Cocrystal Structures of BjaI Identify the Ligand-Binding Sites. To delineate the binding pockets for both substrates SAM and isovaleryl–CoA, we determined the crystal structures of BjaI in complex with various combinations of ligands (see *SI Appendix*, Table S4, for relevant statistics). The core structure of BjaI represents a distal subclade of the GNAT superfamily, despite a lack of any notable sequence similarities between the AHL synthases and GNAT enzymes (32). The overall topology consists of a central core of seven β-strands, flanked by α-helices, and defines the protein fold as a phosphopantetheine-binding domain (Fig. 3*A*). A structure-based search using the DALI server (33) identifies the closest structural homologs as the ACP-dependent AHL synthases LasI (PDB Code: 1RO5; rmsd of 2.2 Å over 182 aligned Cα atoms) (28), TofI (PDB Code: 3P2F; rmsd of 2.0 over 167 aligned Cα atoms) (30), and EsaI (PDB Code: 1KZF; rmsd of 2.3 over 169 aligned Cα atoms) (29). While AHL synthases share structural

Table 1. Steady state kinetic parameters for wild-type and variant BjaI

BjaI	k_{cat} (s^{-1}) x 10^{-3}	K_m (M) x 10^{-6}	k_{cat}/K_m ($M^{-1}s^{-1}$) x 10^3
Wild type	45.00 ± 2.67	2.10 ± 0.40	21.43 ± 4.33
Trp34→Ala	1.83 ± 0.10	1.80 ± 0.30	1.02 ± 0.18
Asp46→Ala	2.17 ± 0.33	11.00 ± 2.20	0.20 ± 0.05
Met78→Ala	2.17 ± 0.03	1.80 ± 0.30	1.21 ± 0.20
Trp101→Ala	1.67 ± 0.02	1.90 ± 0.10	0.88 ± 0.05
Trp101→Phe	1.17 ± 0.17	6.00 ± 2.80	0.20 ± 0.10
Arg103→Ala	1.33 ± 0.02	2.00 ± 0.30	0.67 ± 0.08
Tyr104→Ala	1.33 ± 0.08	2.10 ± 0.50	0.63 ± 0.15
Met139→Ala	4.17 ± 0.33	3.40 ± 1.30	1.23 ± 0.48
Trp142→Ala	2.33 ± 0.17	10.10 ± 1.60	0.23 ± 0.05
Trp142→Phe	11.50 ± 5.67	26.00 ± 17.00	0.44 ± 0.37
Trp143→Ala	3.17 ± 0.33	5.40 ± 0.70	0.59 ± 0.10
Trp143→Phe	1.50 ± 0.17	8.00 ± 1.20	0.19 ± 0.03
Phe147→Ala	6.67 ± 0.33	3.90 ± 0.60	1.71 ± 0.28

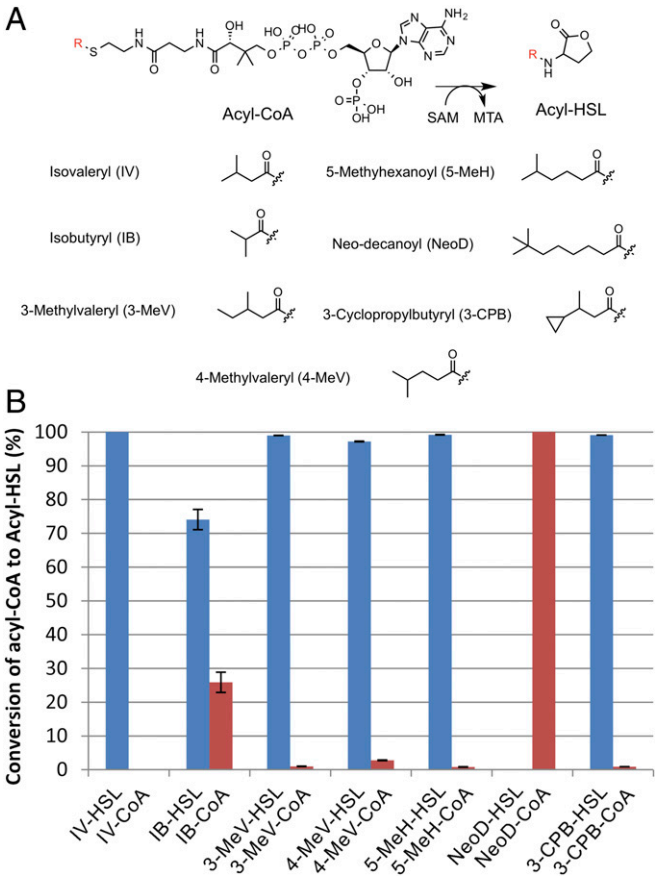

Fig. 2. Substrate scope of BjaI. (*A*) Structures of various branched acyl–CoA produced by semisynthesis. (*B*) End-point liquid-chromatography–mass spectrometric analysis showing the production of acyl–homoserine lactone (in blue) from the corresponding acyl–CoA (in red) using BjaI. Experiments were conducted in triplicate, and error bars represent the SD between measurements.

homology of bona fide *N*-acetyltransferases, the latter enzymes are easily distinguished by their smaller size of roughly 150 residues (34). There are notable differences in the *N*-terminal regions between BjaI and the three other AHL synthases that have been characterized, and this may be reflective of differences in substrate binding between these enzymes (*SI Appendix*, Fig. S13) (35).

The cocrystal structures of BjaI with SAH or MTA define the binding pocket of SAM as a pocket located between helices α1 and α2 and supported by a loop located between strands β6 and β7 (Fig. 3*B*). A comparison of the SAH- and MTA-bound structures of BjaI with that of SAM + isopentyl–CoA reveals a common binding orientation with only a small movement near the sulfur atom, which is necessary to accommodate the methyl group in SAM (Figs. 3 *C*–*E*). The adenine ring is stacked in a hydrophobic pocket and is flanked by residues Thr36 and Leu37 on one side and Met78, Val82, and Phe83 on the other side. The N6 of the adenine is within hydrogen-bonding distance to Asp46, and the O2′ of the ribose is in proximity to Thr36, but the geometry of the interaction is less optimal for hydrogen bonding. The 3-amino–3-carboxylpropyl moiety is stabilized through numerous contacts with the polypeptide, including interactions between the α-amine and the backbone carbonyl oxygen of Ile138, while the α-carboxylate is held in place through interactions with the side chain η1 and backbone amide of Arg103 and side chain of Ser102, respectively. BjaI residues Phe83 and Ile183 direct the orientation of the 3-amino–3-carboxylpropyl into the core of the enzyme, and the 5′-methylthioribose ring is stabilized through a stacking interaction with the side chain of Trp34. Many of these residues are conserved across various AHL synthases. The Asp46→Ala variant has a significant effect on both k_{cat} and K_m, resulting in a near 100-fold decrease in catalytic efficiency (0.20×10^3 $M^{-1}s^{-1}$), while the Met78→Ala variant shows a 20-fold decrease in catalytic efficiency (1.21×10^3 $M^{-1}s^{-1}$), relative to the wild-type enzyme (Table 1 and *SI Appendix*, Fig. S14).

Structures of BjaI with either isovaleryl–CoA or the inert isopentyl–CoA identify the phosphopantetheine and acyl chain-binding pockets, as well as the determinants for phosphoadenosine binding found in the CoA-specific AHL synthases (Figs. 3 *E* and *F*). A prominent feature in BjaI is a β-bulge between two invariants residues, Ser102 and Arg103 in strand β4, which forms the base of a pocket enclosed by strands β4, β5, and β7 and helices α4 and α6. This pocket defines the phosphopantetheine and acyl chain-binding sites, consistent with prior modeling studies on EsaI (29) and structures of TofI bound to a small molecule (30). The oxygen atom of the thioester is within interaction distance from the backbone amides of Arg103 and Tyr104, which presumably stabilizes the oxyanion that is formed during the attack of the SAM α-amine onto the thioester carbon. Both Arg103→Ala and Tyr104→Ala variants displayed over 33-fold slower turnover (k_{cat}) than that of the wild-type BjaI (1.33×10^{-3} s^{-1} vs. 45.00×10^{-3} s^{-1}) (Table 1 and *SI Appendix*, Fig. S14).

Numerous residues interact with the pantothenic acid, including the backbone amide of Asp112 and the side chain of Arg116 with the phosphate and interactions of the two keto oxygen atoms and the backbone amide of Val106 and the side chain of Arg32. The CoA-binding tunnel is lined with numerous hydrophobic residues, including Ile27, Phe28, Trp34, Tyr104, Val106, and Trp143. In the cocrystal structures with MTA or SAH, without any bound CoA, the phosphopantetheine tunnel is partially blocked by the side chain of Arg32. A similar grouping of hydrophobic residues lines the putative phosphopantetheine-binding pockets of LasI, EsaI, and TofI.

Notably, binding of the acyl–CoA is largely supported through π-stacking interactions between the adenine ring and Trp142 located at the beginning of helix α5. The residue, in turn, stacks with the following residue, Trp143, resulting in the formation of an "indole platform" that provides a foundation for binding to the adenine ring

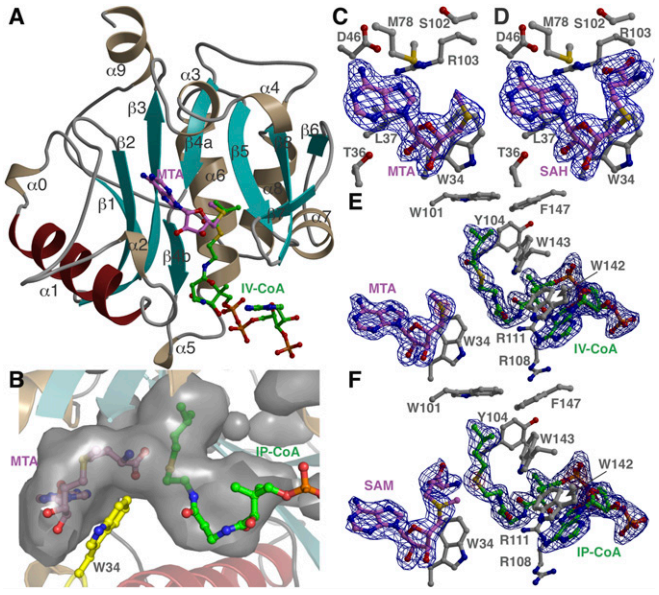

Fig. 3. Cocrystal structures of BjaI. (*A*) Ribbon diagram of BjaI in complex with methyl thioadenosine (MTA, in pink) and isovaleryl–CoA (IV-CoA, in green). Secondary structure elements are demarcated, and helix α1, which is mobile in the absence of nucleotide, is colored in deep red. (*B*) Active-site pocket showing the two cavities that accommodated substrates SAM (in pink) and acyl–CoA (isopentyl–CoA, in green). Trp34 (in yellow) is located adjacent to both cavities. (*C*–*F*) Simulated annealing difference Fourier maps (Fo-Fc) of BjaI complexes contoured to 2.5σ (blue) showing the bound ligands and important active-site residues. Protein residues are shown in gray, MTA/SAM is shown in pink, and the acyl–CoA is shown in green.

of CoA (Figs. 3 *E* and *F*). The Trp142→Ala, Trp142→Phe, Trp143→Ala, and Trp143→Phe variants all demonstrated significant negative effect on both k_{cat} and K_m, resulting in over 93-, 48-, 36-, and 112-fold drops in the catalytic efficiency, respectively (Table 1 and *SI Appendix*, Fig. S14). Two residues, Arg108 and Arg111, located in the loop between strand β4 and helix α4 that is positioned at the opposite periphery from the "indole platform," orientate the pantothenic acid into the enzyme active site. Three of these four residues are conserved across all of the characterized CoA-dependent AHL synthases, with the exception of Arg108, which is a Pro in all other homologs. It is not surprising that these residues are not shared with the ACP-dependent enzymes, which would interact with a protein-linked substrate.

Framework for Understanding Acyl Chain Specificity. The branched 3-methylbutanoic acid moiety in cocrystal structures with isovaleryl–CoA or the inert analog isopentyl–CoA (Fig. 3) establishes the location of the acyl chain-binding site in BjaI. The branched acyl chain is ensconced in a hydrophobic pocket surrounded by enzyme residues Tyr104, Met139, and Trp143. The top of this pocket is closed off by Trp101 and Phe147, providing a rationale for why BjaI cannot use acyl chains that are longer than C7. The Trp101→Ala, Trp101→Phe, Met139→Ala, Trp143→Ala, Trp143→Phe, and Phe147→Ala mutations result in 24, 107, 17, 36, 112, and 12-fold decreases of k_{cat}/K_m values, respectively, relative to wild-type BjaI (Table 1 and *SI Appendix*, Fig. S14). The volume of the binding pocket [136 $Å^3$ as calculated using the CASTp server (36)] is sufficiently wide to accommodate isovalerate, and preference for the branched chain may be due to favorable van der Waals contacts with the residues in this pocket.

A comparison of the BjaI cocrystal structures with those of ligand-free LasI (specific for 3-oxo–C12 HSL), EsaI (specific for 3-oxo–C6 HSL), and the small-molecule–bound structure of TofI (specific for C8 HSL) offers insights into the basis for acyl chain preferences (*SI Appendix*, Fig. S15). A view parallel to the axis of the pantothenic acid and 3-methylbutanoate in the BjaI cocrystal structure shows that many of the residues that line the sides of the acyl chain-binding cavity are either largely conserved or substituted with similar residues in all of the AHL synthase structures. These include Tyr104 (Phe in LasI, EsaI and TofI), Met139 (Thr in LasI, and TofI, and Val in EsaI), and Trp143 (Met in EsaI and TofI, Val in LasI). However, the residues at the top of the pocket are highly divergent, resulting in pockets that vary considerably in volume. For example, the aforementioned Trp101/Phe147 that encapsulates the pocket in BjaI to restrict binding of acyl chains longer than C8 is substituted in each of the other enzymes that use longer chain substrates. In LasI, the Leu102/Met152 pair occupies the equivalent position, resulting in an open binding cavity that is long enough to accommodate the cognate 3-oxo–C12 chain. Similarly, in EsaI the Ser98/Leu150 replacement also opens the cavity, which is terminated by Trp155 to create the binding pocket that is suitable to accommodate the 3-oxo–C6 substrate. Lastly, the Leu102/Phe153 replacement in TofI similarly enlarges the cavity, which is terminated by Trp178 to form a binding pocket suitable for the C8–acyl substrate. Notably, Ala137 in BjaI is an aliphatic residue among all AHL synthases (replaced by either Gly, Val, Ile, or Leu), with the exception of both LasI and EsaI, which contain a Thr at this position. The side chain β-hydroxyl of Thr is well positioned to interact with the oxygen of the β-keto group in each of the corresponding 3-oxo substrates of LasI and EsaI.

The BjaI cocrystal structures reveal that Trp34 is located adjacent to the binding sites for SAM and acyl–CoA, and this residue forms part of the binding platforms for both ligands. The Trp34→Ala mutation in BjaI results in a near 25-fold decrease in k_{cat} (1.83×10^{-3} s^{-1} vs. 4.5×10^{-2} s^{-1} for the wild type) with only a modest effect on K_m (Table 1 and *SI Appendix*, Fig. S14). An equivalent Trp is conserved across all CoA- and ACP-dependent AHL synthases where it is located either in helix α2 or loop that follows. This region of AHL synthases is highly mobile, and the orientation of residues in this region varies considerably among structures of ligand-free AHL synthases. In the LasI structure, the equivalent Trp33 protrudes directly into the SAM-binding pocket (28), while in the EsaI structure Trp34 is displaced nearly 30 Å away into a hydrophobic patch located away from the active site (*SI Appendix*, Fig. S16) (29). To probe the influence of SAM/SAH/MTA binding on BjaI, we probed the sensitivity of the enzyme to treatment with substoichiometric concentrations of the protease trypsin in the presence and absence of MTA (*SI Appendix*, Fig. S17). Notably, binding of SAM results in increased stability of BjaI to protease treatment. Presumably, mobile regions near the binding site become ordered upon SAM binding, which confers the orientation of the region harboring Trp34 to establish the pockets for acyl–CoA/ACP.

Enzyme-Bound Isovalerate–SAH Intermediate. Prior transient-state kinetic data, as well as substrate scope studies, established that formation of the homoserine lactone product occurs through an acyl–SAM intermediate (37). Additionally, initial velocity studies with the ACP-dependent RhlI showed that SAH was a pseudosubstrate that could not undergo acylation, but induced the hydrolysis of the butyryl–ACP substrate (37). The difference in activity was attributed to alterations in binding mode, resulting in a suboptimal orientation of SAH in the enzyme active site. However, as our structural data demonstrate that SAM, SAH, and MTA all bind in essentially identical conformations, we sought to explore whether BjaI was capable of generating an acyl–SAH intermediate. This intermediate lacks a leaving group at the sulfide and, consequently, cannot undergo lactonization. Surprisingly, a time-course analysis of reaction products using isovaleryl–CoA and SAH reveals the buildup of an intermediate with a mass consistent with that of isovaleryl–SAH (Fig. 4*A*).

By carrying out crystallization of BjaI with isovaleryl–CoA and SAH, we were able to determine a 1.8-Å–resolution cocrystal structure with clear and obvious electron density corresponding to isovaleryl–SAH conjugate at the active site (Fig. 4*B*). In the structure, the SAH moiety of the adduct is situated nearly identically with the location of the SAM/MTA, but the isovalerate keto group is shifted 2 Å away to form an amide linkage with the α-amine of SAH. The position of the acyl chain does not shift considerably, consistent with the selectivity of the acyl chain-binding pocket of AHL synthases. The isovaleryl–SAH conjugate is oriented linearly across the two pockets, and, consequently, the carbonyl oxygen shifts still retain interactions with the backbone amides of Arg103 and Tyr104. Notably, a superposition of the isovaleryl–SAH-bound structure with that of SAH alone reveals significant differences in the orientation of the 3-amino–3-carboxylpropyl (Fig. 4*C*). In the isovaleryl–SAH complex, the α-carboxylate oxygen is now positioned to be nearly in line with the sulfur and adjacent methylene carbon and positioned roughly 4.4 Å away from this methylene carbon. In structures with just SAH or SAM, the angle between the α-amine, α-carbon, and α-carboxylate carbon of the ligand is nearly 5° smaller than that for the equivalent atoms in the acyl–SAH complex. The reorganization induced by SAH/SAM acylation may facilitate subsequent lactonization.

Structure-Based Classification of AHL Synthases. To further characterize the diversity of and relationships among AHL synthases, we generated a sequence similarity network using the toolkit provided by the Enzyme Function Initiative (38). Using a default cutoff E value (significance threshold) of 10^{-5} and the primary sequence of BjaI as a seed sequence, a total of 934 sequences were culled from UniProt (represented as circles/nodes in Fig. 5). Each edge connection between two different nodes represents a similarity between the two corresponding protein sequences set to a cutoff value. A sequence alignment cutoff of at least 45% yielded 18 different groups, which clustered almost entirely based on organismal class (Fig. 5*A*). Cluster 1 consists of three subclusters and contains several of the biochemically characterized CoA-dependent AHL synthases, including BjaI (cluster 1a), RpaI, and BraI (both in cluster 1b). A more stringent network with a sequence alignment cutoff of at least 50% yields the network shown in Fig. 5*B*. This network includes all presumed CoA-dependent AHL

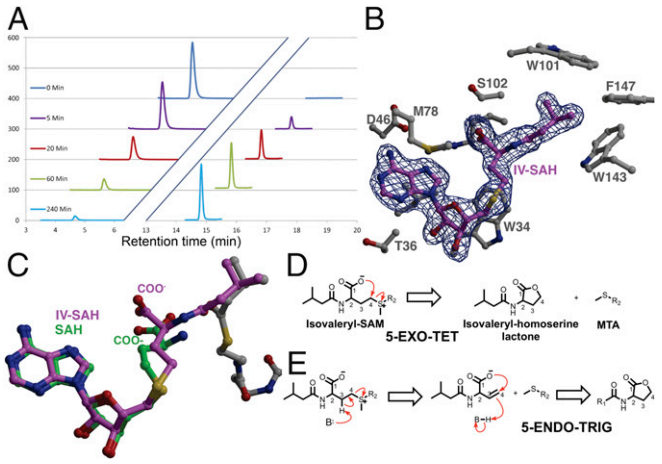

Fig. 4. Observation of the acyl–SAH intermediate. (*A*) HPLC analysis of the reaction time course demonstrating the production of a covalent isovaleryl–SAH intermediate (elution time of 15 min) from SAH (elution time near 5 min). The identity of all products was confirmed by mass spectrometry. (*B*) Simulated annealing difference Fourier maps (Fo-Fc) of BjaI complexes contoured to 2.5σ (blue) showing the bound isovaleryl–SAH intermediate (in pink) and active-site residues (in gray). (*C*) Superposition of the BjaI complex structures with isovaleryl–SAH (in pink) and SAH (in green). Note the change in the orientation of the carboxylate, which would facilitate lactone formation. (*D* and *E*) Proposed mechanisms for the breakdown of the acyl–SAH intermediate to form the lactone product via either a (*D*) concerted S_N2-like mechanism or (*E*) distributive E2-type mechanism. The former mechanism occurs through a more favorable orbital overlap.

synthases, which cluster based on predicted substrate preference (*SI Appendix*, Fig. S18–S21).

To test the hypothesis that nodes in clusters 1c (*SI Appendix*, Fig. S20) and cluster 2 (*SI Appendix*, Fig. S21) represent bona fide CoA-dependent AHL synthases, we carried out biochemical characterization of representative members from each cluster. Notably, sequences in each of these clusters lack the canonical "indole platform" that is necessary for CoA-binding, and sequences on cluster 1c have a Phe/Trp replacement, while the sequences in cluster 2 have a Tyr/Phe replacement (Fig. 5*C*). Putative AHL synthases MesI (from cluster 1c) and MplI (from cluster 2) were heterologously expressed and purified and tested for the ability to generate homoserine lactone products using a CoA tethered acyl substrate in an end-point assay (*SI Appendix*, Fig. S22). To demonstrate that acyl–CoA was the preferred substrate over the corresponding acyl–ACP, we generated octanoyl–ACP and determined the kinetic parameters of MesI for octanoyl–CoA and octanoyl–ACP. A comparison of the kinetic parameters for octanoyl–CoA (k_{cat} = 14.4 × 10^{-3} s^{-1}; K_m = 14.44 × 10^{-6} M; k_{cat}/K_m = 9.97 × 10^2 $M^{-1}s^{-1}$) against those for octanoyl–ACP (k_{cat} = 2.07 × 10^{-3} s^{-1}; K_m = 10.02 × 10^{-6} M; k_{cat}/K_m = 2.07 × 10^2 $M^{-1}s^{-1}$) suggests that the acyl–CoA is the preferred substrate for MesI (Fig. 5*D*). The difference in efficiency for the acyl–CoA substrate relative to the acyl–ACP is roughly comparable in range to that observed for the ACP-dependent AHL synthase RhlI using a CoA-linked substrate (39). These data suggest that a canonical "indole platform" is not a strict requirement for acyl–CoA utilization.

Discussion

Multiple sequence alignments of LuxI-type enzyme with different acyl chain specificities had identified several conserved residues located in four blocks, which are presumed to function in recognition of SAM and/or ACP (27, 35). The function of each of these residues, which constitute the "sequence signatures" of AHL synthases, can be reconciled in the context of the structures and associated data presented here. The first block contains the strictly conserved Arg22, Phe28, and Trp34 located in helix α2 and the following loop. This region is highly mobile in the absence of SAM, and binding of this ligand fixes the location of these residues, including Trp34 that defines the base of the acyl chain-binding pocket. The second and third signature blocks consist of residues Asp46, Asp49, Arg69, and Arg103, and these residues are all located in the proximity of the adenine ring of the bound SAM, although only Asp46 and Arg103 are within contact distance of the base. A fifth conserved residue in this block, Glu100, is essential for AHL synthesis by LuxI and RhlI and had been postulated to serve as the general base that abstracts a proton from the SAM α-amine before nucleophilic attack. However, our structural data argue against this notion based on the 8-Å distance of this residue from SAM. In contrast, Glu140 is located only 4 Å away, suggesting that Glu140 may serve as the general base. Alternatively, the pK_a of the α-amine may be perturbed in the enzyme active site, negating the requirement for an active-site general base. The fourth signature block is more divergent and consists of several residues that line the periphery of the acyl chain-binding pocket, including Met139 and Trp143. Notably, Thr142 of LasI and Thr140 in EsaI occupy a location that is normally a small aliphatic residue in most other AHL synthases, and mutational analysis of EsaI suggests that the Thr accounts for the altered preference for substrates with oxidation at the β-carbon. The BjaI cocrystal structures support the role for a Thr at this position for recognition of 3-oxo substrates.

The biosynthetic activity of the ACP-dependent AHL synthases requires a substrate bound to a protein cofactor, and a putative binding site for the ACP has been proposed based on modeling studies (28). As most protein interactions with ACPs are mediated through electrostatics, a putative binding site was identified in LasI near a region clustered with several basic residues, including Arg154, Arg161, Lys167, and Arg172, most of which are conserved across other ACP-dependent synthases (*SI Appendix*, Fig. S13).

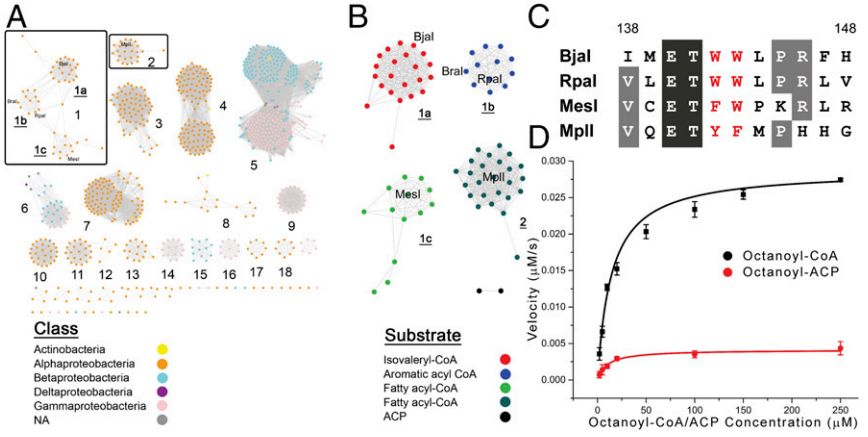

Fig. 5. Structure-based classification of AHL synthases. (*A* and *B*) Sequence similarity network illustrating the relationship among different AHL synthases. (*A*) Alignment cutoff of at least 45% yielded 18 different groups, which clustered almost entirely based on organismal class, while (*B*) a more stringent cutoff of at least 50% yields the network that is clustered based on predicted substrate preference. The CoA-dependent AHL synthases can be further subdivided into four clades based on the CoA-linked acyl donor. (*C*) Divergence in sequence among the different CoA-dependent clade sequences near the "indole platform." (*D*) Michaelis–Menten curve obtained by measuring CoA production by MesI over varying concentrations of either octanoyl–CoA (black curve) or octanoyl–ACP (red curve), at a fixed concentration of 1 mM *S*-adenosylmethionine.

Mutational analysis confirms a role for several of these residues in catalysis, presumably via engagement of the ACP (28). The equivalent residues in BjaI are not cationic, but are located directly adjacent to the phosphoadenosine, providing further support of the modeling and mutational studies.

The cocrystal structure of BjaI in complex with isovaleryl–SAH reveals a reorganization of the 3-amino–3-carboxylpropyl likely occurs following acylation, resulting in a near-5° increase in the bond angle at the α-carbon. This reorganization is due to the loss of favorable electrostatic interactions between the negatively charged carboxylate and the positively charged amino group of SAM upon formation of the acyl–SAM, which does not contain a charged amine. Consequently, acylation activates the substrate for lactonization by positioning the attacking carboxylate oxygen toward the methylene carbon adjacent to the sulfur to facilitate ring closure. Lactone formation can occur through an S_N2-type direct nucleophilic attack of the carboxyl oxygen onto the methylene or through an E2-type β-elimination of MTA, followed by an attack of the carboxyl oxygen on the resultant vinyl moiety. As postulated by Tipton and colleagues (37), the Baldwin rules for ring closure for an S_N2 mechanism would occur through a favored 5-exo–tet closure, while the E2-type mechanism would invoke an unfavorable 5-endo–trig reaction (Fig. 4*D*). The BjaI acyl–SAH cocrystal structure illustrates how acylation of SAM/SAM could precipitate ring formation through the proper positioning of nucleophile, electrophile, and leaving group.

The identification of small molecules that can divert quorum signaling has spurred a renewal in quorum-sensing pharmacology (40). Compounds that mimic the acyl chain of cognate substrates are poor competitive inhibitors of AHL synthases, as are acyl–SAM analogs. Our studies here suggest that formation of a competent acyl chain-binding pocket only fully occurs following the reorganization of Trp34 induced by the binding of SAM, and acylated mimics would likely not bind in a productive fashion. This point is further reinforced by the observation that the cyclic ketone of J8-C8 (30), which is presumed to mimic the lactone of AHLs, is bound by TofI at a site that is different from the AHL pocket identified in this work. Our studies suggest that mechanism-based inhibitors of AHL synthases that cannot undergo lactone formation may prove to be a suitable class of small-molecule inhibitors for the pharmaceutical intervention of quorum signaling.

Materials and Methods

Detailed methods for protein expression, purification, chemical synthesis, biochemical, and crystallographic studies can be found in *SI Appendix*.

ACKNOWLEDGMENTS. We thank Keith Brister and colleagues for facilitating data collection at the Life Sciences Collaborative Access Team (Argonne National Laboratories, IL). We also thank Dr. Vinayak Agarwal (University of California, San Diego) for providing overexpression constructs for CoA, CoaD, and CoE and Dr. Jian Min (University of Illinois) for helpful discussions about CoA precursor synthesis. Q.H.C. and E.P.G. are supported by NIH Grant GM59026. R.N. is supported by NIH grant GM117323. All NMR data were collected at the facility in the Mining Microbial Genomes theme of the Carl R. Woese Institute for Genomic Biology.

1. Rutherford ST, Bassler BL (2012) Bacterial quorum sensing: Its role in virulence and possibilities for its control. *Cold Spring Harb Perspect Med* 2:a012427.
2. Schuster M, Sexton DJ, Diggle SP, Greenberg EP (2013) Acyl-homoserine lactone quorum sensing: From evolution to application. *Annu Rev Microbiol* 67:43–63.
3. Bandara HM, Lam OL, Jin LJ, Samaranayake L (2012) Microbial chemical signaling: A current perspective. *Crit Rev Microbiol* 38:217–249.
4. Davies DG, et al. (1998) The involvement of cell-to-cell signals in the development of a bacterial biofilm. *Science* 280:295–298.
5. Zhu J, et al. (2002) Quorum-sensing regulators control virulence gene expression in Vibrio cholerae. *Proc Natl Acad Sci USA* 99:3129–3134.
6. Koutsoudis MD, Tsaltas D, Minogue TD, von Bodman SB (2006) Quorum-sensing regulation governs bacterial adhesion, biofilm development, and host colonization in Pantoea stewartii subspecies stewartii. *Proc Natl Acad Sci USA* 103:5983–5988.
7. Atkinson S, Chang CY, Sockett RE, Cámara M, Williams P (2006) Quorum sensing in Yersinia enterocolitica controls swimming and swarming motility. *J Bacteriol* 188:1451–1461.
8. LaSarre B, Federle MJ (2013) Exploiting quorum sensing to confuse bacterial pathogens. *Microbiol Mol Biol Rev* 77:73–111.
9. Li Z, Nair SK (2012) Quorum sensing: How bacteria can coordinate activity and synchronize their response to external signals? *Protein Sci* 21:1403–1417.
10. Kaplan HB, Greenberg EP (1985) Diffusion of autoinducer is involved in regulation of the Vibrio fischeri luminescence system. *J Bacteriol* 163:1210–1214.
11. Pearson JP, Van Delden C, Iglewski BH (1999) Active efflux and diffusion are involved in transport of Pseudomonas aeruginosa cell-to-cell signals. *J Bacteriol* 181:1203–1210.
12. Fuqua WC, Winans SC, Greenberg EP (1994) Quorum sensing in bacteria: The LuxR-LuxI family of cell density-responsive transcriptional regulators. *J Bacteriol* 176:269–275.
13. Fuqua C, Greenberg EP (2002) Listening in on bacteria: Acyl-homoserine lactone signalling. *Nat Rev Mol Cell Biol* 3:685–695.
14. Parsek MR, Greenberg EP (2000) Acyl-homoserine lactone quorum sensing in gram-negative bacteria: A signaling mechanism involved in associations with higher organisms. *Proc Natl Acad Sci USA* 97:8789–8793.
15. Swift S, Throup JP, Williams P, Salmond GP, Stewart GS (1996) Quorum sensing: A population-density component in the determination of bacterial phenotype. *Trends Biochem Sci* 21:214–219.
16. Bassler BL, Wright M, Showalter RE, Silverman MR (1993) Intercellular signalling in Vibrio harveyi: Sequence and function of genes regulating expression of luminescence. *Mol Microbiol* 9:773–786.
17. Hanzelka BL, et al. (1999) Acylhomoserine lactone synthase activity of the Vibrio fischeri AinS protein. *J Bacteriol* 181:5766–5770.
18. Laue BE, et al. (2000) The biocontrol strain Pseudomonas fluorescens F113 produces the Rhizobium small bacteriocin, N-(3-hydroxy-7-cis-tetradecenoyl)homoserine lactone, via HdtS, a putative novel N-acylhomoserine lactone synthase. *Microbiology* 146:2469–2480.
19. Burton EO, Read HW, Pellitteri MC, Hickey WJ (2005) Identification of acyl-homoserine lactone signal molecules produced by Nitrosomonas europaea strain Schmidt. *Appl Environ Microbiol* 71:4906–4909.
20. Moré MI, et al. (1996) Enzymatic synthesis of a quorum-sensing autoinducer through use of defined substrates. *Science* 272:1655–1658.
21. Schaefer AL, Val DL, Hanzelka BL, Cronan JE, Jr, Greenberg EP (1996) Generation of cell-to-cell signals in quorum sensing: Acyl homoserine lactone synthase activity of a purified Vibrio fischeri LuxI protein. *Proc Natl Acad Sci USA* 93:9505–9509.
22. Raychaudhuri A, Jerga A, Tipton PA (2005) Chemical mechanism and substrate specificity of RhlI, an acylhomoserine lactone synthase from Pseudomonas aeruginosa. *Biochemistry* 44:2974–2981.
23. Lindemann A, et al. (2011) Isovaleryl-homoserine lactone, an unusual branched-chain quorum-sensing signal from the soybean symbiont Bradyrhizobium japonicum. *Proc Natl Acad Sci USA* 108:16765–16770.
24. Schaefer AL, et al. (2008) A new class of homoserine lactone quorum-sensing signals. *Nature* 454:595–599.
25. Ahlgren NA, Harwood CS, Schaefer AL, Giraud E, Greenberg EP (2011) Aryl-homoserine lactone quorum sensing in stem-nodulating photosynthetic bradyrhizobia. *Proc Natl Acad Sci USA* 108:7183–7188.
26. Christensen QH, Brecht RM, Dudekula D, Greenberg EP, Nagarajan R (2014) Evolution of acyl-substrate recognition by a family of acyl-homoserine lactone synthases. *PLoS One* 9:e112464.
27. Parsek MR, Schaefer AL, Greenberg EP (1997) Analysis of random and site-directed mutations in rhlI, a Pseudomonas aeruginosa gene encoding an acylhomoserine lactone synthase. *Mol Microbiol* 26:301–310.
28. Gould TA, Schweizer HP, Churchill ME (2004) Structure of the Pseudomonas aeruginosa acyl-homoserinelactone synthase LasI. *Mol Microbiol* 53:1135–1146.
29. Watson WT, Minogue TD, Val DL, von Bodman SB, Churchill ME (2002) Structural basis and specificity of acyl-homoserine lactone signal production in bacterial quorum sensing. *Mol Cell* 9:685–694.
30. Chung J, et al. (2011) Small-molecule inhibitor binding to an N-acyl-homoserine lactone synthase. *Proc Natl Acad Sci USA* 108:12089–12094.
31. Montebello AN, et al. (2014) Acyl-ACP substrate recognition in Burkholderia mallei BmaI1 acyl-homoserine lactone synthase. *Biochemistry* 53:6231–6242.
32. Dyda F, Klein DC, Hickman AB (2000) GCN5-related N-acetyltransferases: A structural overview. *Annu Rev Biophys Biomol Struct* 29:81–103.
33. Holm L, Laakso LM (2016) Dali server update. *Nucleic Acids Res* 44:W351-5.
34. Churchill ME (2006) A new GNAT in bacterial signaling? *Structure* 14:1342–1344.
35. Hanzelka BL, Stevens AM, Parsek MR, Crone TJ, Greenberg EP (1997) Mutational analysis of the Vibrio fischeri LuxI polypeptide: Critical regions of an autoinducer synthase. *J Bacteriol* 179:4882–4887.
36. Dundas J, et al. (2006) CASTp: computed atlas of surface topography of proteins with structural and topographical mapping of functionally annotated residues. *Nucleic Acids Res* 34:W116-8.
37. Raychaudhuri A, Tullock A, Tipton PA (2008) Reactivity and reaction order in acyl-homoserine lactone formation by Pseudomonas aeruginosa RhlI. *Biochemistry* 47:2893–2898.
38. Gerlt JA, et al. (2015) Enzyme Function Initiative-Enzyme Similarity Tool (EFI-EST): A web tool for generating protein sequence similarity networks. *Biochim Biophys Acta* 1854:1019–1037.
39. Parsek MR, Val DL, Hanzelka BL, Cronan JE, Jr, Greenberg EP (1999) Acyl homoserine-lactone quorum-sensing signal generation. *Proc Natl Acad Sci USA* 96:4360–4365.
40. Christensen QH, Grove TL, Booker SJ, Greenberg EP (2013) A high-throughput screen for quorum-sensing inhibitors that target acyl-homoserine lactone synthases. *Proc Natl Acad Sci USA* 110:13815–13820.